



Modelling of Capillary Pressure-driven Water Flow in Unsaturated Concrete Using Coupled DEM/CFD Approach

Marek Krzaczek^(✉), Michal Nitka, and Jacek Tejchman

Gdańsk University of Technology, Gdańsk, Poland

marek.krzaczek@pg.edu.pl

Abstract. A novel coupled approach to modelling capillary-driven two-phase water flow in unsaturated concrete was formulated. By merging the discrete element method (DEM) with computational fluid dynamics (CFD) under isothermal settings, the process was numerically studied at the me-so-scale in two-dimensional conditions. Small concrete specimens of a simplified particle meso-structure were subjected to fully coupled hydro-mechanical simulation tests in isothermal conditions. A simple uniaxial compression test was used to calibrate the pure DEM represented by bonded spheres, while permeability and sorptivity tests for an assembly of bonded spheres were used to calibrate the pure CFD. For simplified specimens of the pure mortar, mortar with aggregate, and mortar with aggregate and interfacial transition zone (ITZ) of a given thickness, DEM/CFD simulations were performed sequentially. The numerical results of permeability and sorptivity were compared to the data found in the literature. The primary purpose of the re-search was to demonstrate the impact of ITZ on fluid flow in unsaturated concrete caused by capillary pressure.

Keywords: DEM-CFD · Capillary flow · Concrete

1 Introduction

At the meso-scale, aggregates, cement matrix, interfacial transition zones (ITZs) between aggregates and mortar, and macro-pores make up concrete, which is a highly heterogeneous, discontinuous, and porous composite material. ITZs are seen near aggregates and suggest significant compositional changes when compared to the mortar matrix [1]. They have more and larger pores, smaller particles, and less anhydrous cement and C-S-H (calcium silicate hydrate) gel than the cement matrix, resulting in higher transport characteristics (permeability, diffusivity, and conductivity) [2]. They make it easier for external aggressive substances to penetrate concretes, causing both the concrete and the reinforcing to deteriorate. They also help to transmit humidity through concrete. Concrete pores range in size from a few tenths of nanometers to several tens of micrometers. Water may be absorbed into concrete by capillary forces emerging from

the contact of very small pores with a liquid phase if the moisture content inside the concrete is less than its saturation threshold. This is a common water flow mechanism in concrete that is observed in field applications that are subjected to wetting and drying cycles.

The current work shows how to model viscous and capillary-driven two-phase fluid flow in unsaturated uncracked concrete at the meso-scale under isothermal conditions using a novel mathematical mesoscopic approach. Aggregates and ITZs were explicitly considered in the model. Numerical models are especially effective for isolating and quantifying the effect of various parameters on transport qualities that are difficult to get from experimentation. They are also significantly more efficient and cost-effective. At the meso-scale of concrete, numerical simulations were carried out using a fully coupled 2D DEM/CFD technique that included solid mechanics and fluid mechanics (DEM—discrete element method, CFD—computational fluid dynamics). Because a thorough understanding of pore-scale behaviour is required for accurate interpretation and prediction of macroscopic behaviour, DEM was used to capture concrete's mechanical behaviour, and CFD was used to describe the laminar viscous two-phase liquid/gas flow in pores between the discrete elements by employing a channel network, because an understanding of pore-scale behaviour is essential for successful interpretation and prediction of macroscopic behaviour. The pure DEM was represented in simplification by spheres of various diameters and calibrated using a standard uniaxial compression test, whereas the pure CFD was calibrated using a standard permeability (a measure of a material's ability to transmit fluid) and sorptivity (a measure of a material's capacity to absorb/desorb liquid by capillarity) test.

The main purpose of our simulations was to demonstrate the effect of ITZs on fluid flow in unsaturated concretes, which is influenced by both hydraulic and capillary pressure and is difficult to assess empirically. Unsaturated specimens of a simplified meso-structure emulating the pure mortar, mortar including aggregate, and mortar including aggregate with ITZ of a given thickness were subjected to fully coupled hydro-mechanical modeling tests. The interfacial tension, contact angle, and throat radius were used to compute the capillary pressure. The impact of external load direction, water saturation volume, and gas-phase content on fluid flow patterns was also investigated. The numerical results of permeability and sorptivity were compared to published data. Previously, the authors' fully coupled DEM/CFD model was effectively applied to simulate a hydraulic fracturing process in rocks with one- or two-phase fracturing laminar viscous fluid flow made up of a liquid/gas mixture [3, 4].

2 DEM for Cohesive-Frictional Materials

For DEM calculations, the 3D spherical explicit discrete element open code YADE [5] was utilized. The method allows for a small overlap between two touched bodies (the so-called soft-particle model). As a result, an arbitrary micro-porosity can be created using DEM. The model assumes a cohesive bond at the grain contact that fails brittle under the critical normal tensile load [6]. Under normal compression, shear cohesion failure causes contact slip and sliding, which follows the Coulomb friction law. If a cohesive joint between spheres vanishes after reaching a critical threshold, damage occurs. If

any contact between spheres emerges after a failure, the cohesion does not reappear. In quasi-static analyses, a simple local non-viscous dampening is utilized to accelerate convergence. The DEM model does not take into account material softening. Bond damage in tension is the most important micro-scale process for damage in the pre-failure regime (although bonds can also break by shear). For DEM simulations, five key local material parameters are required: E_c (elastic modulus of the grain contact), ν_c (Poisson's ratio of the grain contact), μ (the Coulomb inter-particle friction angle), C_c (cohesive contact force) and T_c (tensile contact force). Furthermore, particle radii R , particle mass density ρ , and damping parameter α_d must be known. The particle breakage was ignored. The material constants are generally identified in DEM using simple laboratory experiments on the material (uniaxial compression, uniaxial tension, shear, biaxial compression). The detailed calibration procedure for frictional-cohesive materials was described in [6–8], and it was based on real simple standard laboratory tests (uniaxial compression and uniaxial tension) of concrete specimens by running several DEM simulations of experiments on discrete element specimens. DEM was shown to be useful for local and global simulations of macro- and micro-cracks in concrete under bending (2D and 3D studies), uniaxial compression (2D and 3D simulations), and splitting tension (2D analyses) [6–8].

3 CFD Model

The authors' paper [4] provided detailed descriptions of the 2D laminar two-phase fluid flow model and a coupling scheme. Two domains coexisted in the original system: a 3D discrete domain (spheres) and a 2D fluid domain (continuum represented by a grid of channels). A grid was used to separate the fluid and solid domains. As a result, each pore was divided into a number of triangles (VP). The gravity centers of the mesh triangles (VP) in the continuous domain between the discrete elements were connected by channels composed of two parallel plates that created a virtual network of pores (VPN) to properly reproduce their changing geometry (shape, surface and position). Two types of channels are introduced [3, 4]: (1) channels between spheres in contact (referred to as virtual channels to mimic real flow in 3D,) and (2) channels connecting grid triangles in pores (referred to as actual channels). The hydraulic aperture (height) of virtual channels was assumed a function of the hydraulic aperture for the infinite normal stress, the hydraulic aperture for the zero normal stress, the effective normal stress at the particle contact and the aperture coefficient [3]. The hydraulic aperture of actual channels was related to the geometry of the neighbouring triangles, and included also a reduction factor to keep the maximum Reynolds number along the primary flow channel below the critical value for laminar flow at all times [3]. Triangles, by definition, had no fluid flow. VPs stored fluid phase fractions and densities as well as accumulating pressure. The density change in a fluid phase caused pressure variations, which was related to the mass change in VPs. In triangles, the momentum conservation equation was thus ignored, but the mass was still conserved throughout the full volume of triangles. The density of fluid phases contained in VPs was calculated using state and continuity equations. The fluid phase fractions in VPs were computed using the continuity equation for each phase, with the assumption that all fluid phases had the same pressure. The fluid flow in channels

was calculated by solving continuity and momentum equations for incompressible fluid laminar flow. Initially, the liquid and gas may exist in virtual pores. The key fluid flow mechanisms in capillary-driven water flow calculations were piston displacement, snap-off physics, and viscous flow. The cooperative pore filling effect was indirectly taken into account due to the discretization of a single pore. The liquid phase was thought to be a wetting (invading) fluid, while the gas phase was thought to be non-wetting (defending). There were three flow regimes: (a) single-phase gas flow, (b) single-phase liquid flow, and (c) two-phase (liquid and gas) flow. When VP was totally pre-filled with a liquid (wetting) phase and was close to VP, capillary pressure was only evaluated in the flow regime (b). The Washburn equation [9] was used with the Poiseuille equation to link viscous and capillary forces. As a result, for the flow regime (single-phase flow) through channels (capillaries), the mass flow rate of the capillary-driven flow along channels was calculated.

$$M_x = \rho \frac{h^3}{12\mu} \frac{P_i - P_j - P_c}{L} \quad (1)$$

where M_x —the mass fluid flow rate (per unit length) across the film thickness in the x -direction [kg/(m s)], h —the hydraulic channel aperture (its perpendicular width) [m], ρ —the fluid density [kg/m³], t —the time [s], μ —the dynamic fluid (liquid or gas) viscosity [Pa s] and P —the fluid pressure [Pa], P_i and P_j are the pressure in adjacent VPs [Pa], P_c is the capillary pressure [Pa] and L is the length of the channel connecting VPs [m]. Young-Laplace law gives the capillary pressure P_c due to the interface between the two phases (a meniscus).

$$P_c = \frac{2\sigma \cos \Theta}{r_t} \quad (2)$$

where σ is the interfacial tension [N/m], Θ is the contact angle [deg] and r_t is the throat radius equal to half the channel aperture [m]. The coupled DEM-CFD model was implemented into the open-source code YADE [5]. The model has 6 constants for the liquid, 5 for the gas and 6 for the liquid flow network.

4 Model Calibration

A simple uniaxial compression test was used to calibrate the pure DEM represented by spheres, while permeability and sorptivity tests for an assembly of bonded spheres were used to calibrate the pure CFD. In contrast to our prior thorough 3D simulations [6], a simplistic 2D DEM mesoscopic structure was chosen to replicate the mortar/concrete in the first calculation step. Only spheres were chosen as discrete elements. 400 spheres were integrated in a tiny bonded granular specimen of 10×10 mm². Along with the specimen depth, one layer of spheres was applied. The sphere diameter was in the range of 0.25–0.75 mm (with $d_{50} = 0.5$ mm as the mean value). For the sake of simplicity, the macro-pores were ignored. In all simulations, the same simplified concrete meso-structure was assumed. Three different bonded granular specimens were used in the DEM/CFD calculations (Fig. 1): (1) a pure mortar specimen (also known as one-phase concrete), (2) a mortar specimen with one aggregate (also known as two-phase concrete),

and (3) a mortar specimen with one aggregate with ITZ surrounding it (also known as three-phase concrete). The free region between the spheres was represented by micropores. A rigid non-breakable cluster made up of 12 spheres was used to mimic a non-spherical aggregate. ITZ was considered to have three layers of $d = 0.25$ mm spheres around the aggregate with a porosity of $p = 20\%$ (the mortar had a porosity of $p = 5\%$). Experiments [11] were used to calculate the starting porosities of the cement matrix (5%) and ITZ (20%). The width of ITZ was in simulations around 0.75 mm, which was 10 times higher than in real concrete.

In all DEM specimens, the following material constants were used: $E_c = 16.8$ GPa, $\nu_c = 0.20$, $C_c = 180$ MPa and $T_c = 28$ MPa ($C_c/T_c = 5.5$), $\mu = 18^\circ$ and $\rho = 2600$ kg/m³. Previous computations [6–8] calibrated on uniaxial compression, tension, and bending tests were used to choose those values. The results were unaffected by the estimated damping parameter $\alpha_d = 0.20$. The specimen's bottom and top were both smooth. Based on early calculations, a time step of 5×10^{-8} s was assumed. All numerical curves behaved too linearly in a pre-peak region and were too brittle after the peak stress due to large simplifications considered in 2D calculations. The pure mortar with one aggregate had the highest strength, whereas the mortar with one aggregate concrete including ITZ had the lowest. The computed maximum compressive normal stress varied between 52 MPa and 62 MPa. The failure mode was defined by one nearly vertical macro-crack and a few minor vertical and skew cracks.

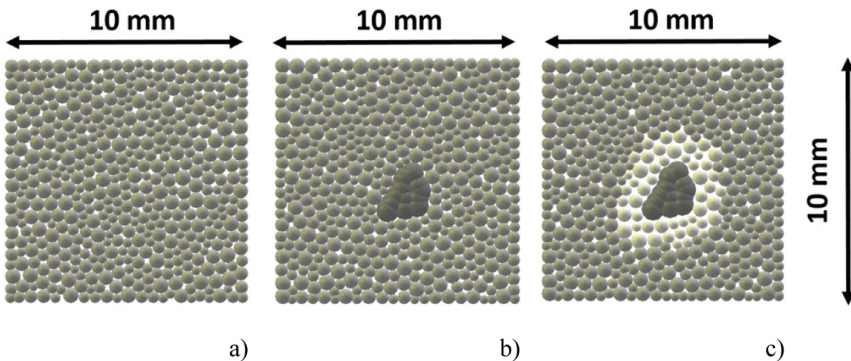


Fig. 1. Numerical specimens in DEM/CFD calculations: (a) pure mortar (grey colour) with initial porosity $p = 5\%$, (b) mortar including aggregate (dark grey colour) with initial porosity $p = 5\%$ and (c) mortar including aggregate with initial porosity $p = 5\%$ and ITZ layer around it (light grey colour) with initial porosity $p = 20\%$

The calibration process of the fluid flow model was split into two parts: (1) permeability tests (Darcy test) and (2) sorptivity tests. A simple permeability Darcy test with two mortar specimens of Fig. 1a was performed for calibration purposes of the CFD model. Single-phase flow was assumed. Two 2D DEM specimens with different initial porosity were prepared. Their size was again 10×10 mm². The first specimen

'1' simulated the mortar and had the initial porosity of $p = 5\%$ and the second specimen '2' simulated ITZ around aggregates and had the initial porosity of $p = 20\%$. The bottom edge was subjected to a constant water pressure of 4.0 MPa, while the top edge was subjected to a constant water pressure of 1.0 MPa. The zero-flux conditions were applied at the left and right edges. For the reference pressure $P_0 = 0.1$ MPa, the dynamic viscosity of water was $\mu = 10.02 \cdot 10^{-4}$ Pa s, its compressibility 10^{-10} Pa⁻¹, and its density $\rho_0 = 998.321 \frac{\text{kg}}{\text{m}^3}$. The virtual channel apertures were $h_{inf} = 4.5 \cdot 10^{-8}$ m and $h_0 = 3.25 \cdot 10^{-6}$ m, respectively. In actual channels, the reduction factor was equal to $\gamma = 0.012$, and the aperture coefficient was equal to $\square\square 1.0$. Both factors γ and \square were multiplied by the same channel aperture factor hc to mimic the differing permeability. The macroscopic permeability coefficient κ was determined using Darcy's law, assuming that the volumetric flow rate at horizontal walls was the same at equilibrium. The findings of the permeability tests differed depending on the channel aperture factor ch ($ch = 1-6$ and 20). The more porous specimen '2' has a higher estimated permeability coefficient of concrete. It ranged from $2e-17$ m² to $3.8e-14$ m² for the specimen '1' ($p = 5\%$) and from $2e-16$ m² to $2e-13$ m² for the specimen '2' ($p = 20\%$). For the subsequent numerical tests, a permeability coefficient of $\kappa = 4e-16$ m² was assumed for the mortar and of $\kappa = 4e-15$ m² for ITZ (10-times lower). Both predicted values were similar to the permeability of cement pastes without and with ITZ (water/cement ratio of 0.5, hydration duration of 28 days, water saturation degree of 0.95), which was determined using a DEM-based technique [2] that was calibrated using experiments (e.g. [12, 13]). In the sorptivity test, the dry porosity 5% specimen was employed. The initial pressure of the fluid (gas phase) was 0.1 MPa. At the bottom specimen edge, constant pressure of 0.14 MPa was used as a boundary condition to fill up the pores in contact with water. The boundary pressure maintains a small pressure gradient on the boundary simulating a slight fluid flow, replenishing the water in the specimen. A constant pressure of 0.10 MPa was defined at the specimen's upper edge. Along the specimen's vertical edges, no mass flow rate was defined. The simulations were run at a temperature of 293.16 K in isothermal circumstances. The calculated sorptivity of the mortar specimen was 0.405 mm/min^{1/2}, being in agreement with laboratory test results [14].

5 Results of Capillary-Driven Fluid Flow in Mortar

Three of the bonded granular specimens from Fig. 1 were chosen for capillary-driven fluid flow testing once more. For all specimens, the initial and boundary conditions were the same. The fluid's initial pressure (gas and liquid phase) was set to 0.1 MPa (close to the atmospheric pressure). The liquid fraction was 97% and the gas fraction 3%. A constant pressure of 0.14 MPa was chosen to replicate the pore filling with water. The boundary pressure maintained a small pressure gradient on the boundary simulating a minor fluid flow, replenishing the water in the specimen (it was defined in pores in contact with the specimen bottom). Before the capillary pressure became effective, this pressure was slightly greater than the initial pressure in the fluid domain (0.1 MPa) to fill in the pores with water. A mass flux rate of zero was defined along the remaining specimen boundaries. As a result, the capillary pressure was the primary driver of fluid flow. The transient process occurred in an isothermal environment. In the solid-fluid realm,

a constant and uniform temperature of 293.16 K was established. The distribution of the capillary pressure, water phase fraction, water saturation state and high hydraulic pressure zone in 3 specimens of Fig. 1 are presented in Figs. 2, 3 and 4.

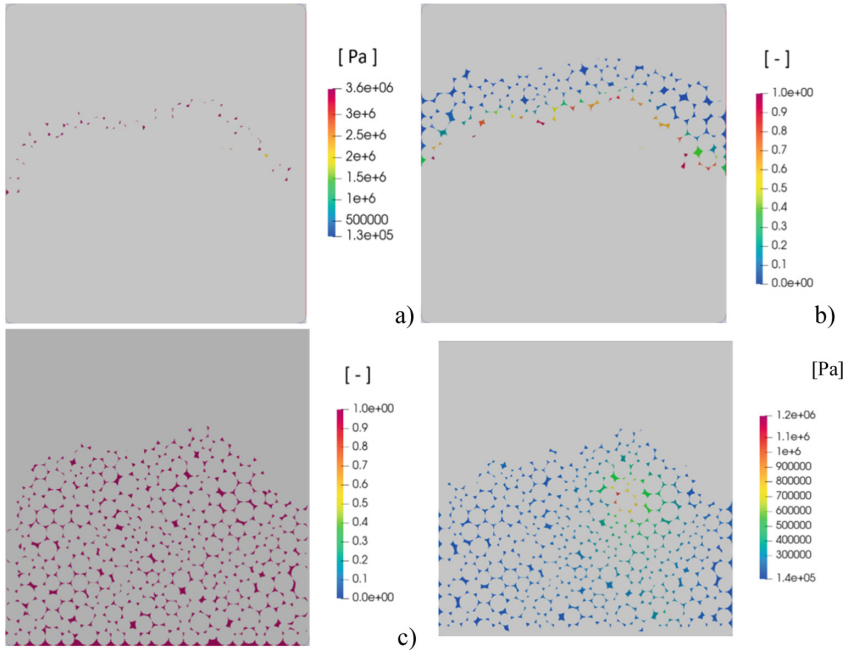


Fig. 2. Computation results of capillary-driven fluid flow in mortar specimen: (a) capillary pressure, (b) water phase fraction, (c) water saturation state and (d) high hydraulic pressure zone

The coupled DEM-CFD calculation results show that the maximum capillary pressure was $P_{cmax} = 3.6$ MPa. The sorptivity by Hall [14] was 0.405 mm/min^{1/2} (mortar), 0.401 mm/min^{1/2} (mortar + aggregate) and 0.276 mm/min^{1/2} (concrete). It was reduced by the presence of both the barrier in the form of the aggregate and porous ITZ. The height of the full saturation area was reduced by ITZ due to its high porosity. The high liquid phase fraction and the high hydraulic pressure dominated in ITZ.

It can be concluded that ITZs in concrete decelerate the capillary fluid flow and consequently reduce sorptivity. In unsaturated concretes, however, the hydraulic pressure, not the capillary pressure, becomes the major component driving fluid flow when the hydrostatic pressure of water on the outer surface of a structural element constructed of concrete is sufficiently high. Because ITZs have a higher permeability than the cement matrix, they speed up the fluid movement and the process of filling the pores with water.

6 Summary and Conclusions

A new hydro-mechanical DEM/CFD model of multi-phase fluid flow in unsaturated concretes under isothermal conditions is proposed in this paper. The model allows for

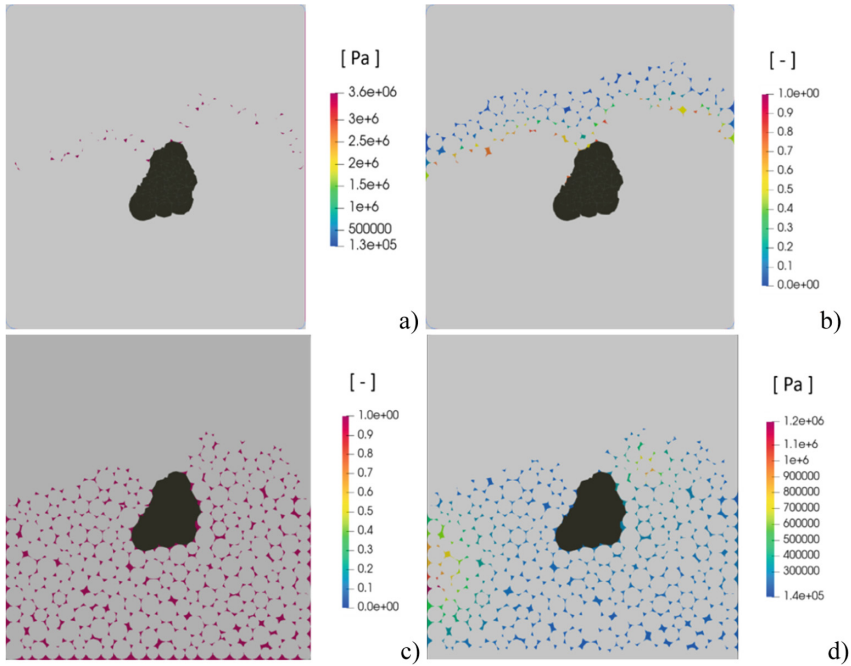


Fig. 3. Computation results of capillary-driven fluid flow in mortar specimen with aggregate: (a) capillary pressure, (b) water phase fraction, (c) water saturation state and (d) high hydraulic pressure zone

the precise tracking of liquid/gas fractions in pores and cracks, including their geometry, topology, size, and location. The results of the model help to clarify the impacts of ITZ on water transport through cementitious materials. Our numerical investigations on permeability and sorptivity of cement matrices and concretes have led us to the following main conclusions:

Porous ITZs in concretes reduce sorptivity by slowing the capillary fluid flow. In unsaturated concretes, sufficiently high hydraulic water pressures become the major factor driving fluid movement. Porous ITZs speed the full saturation of pores in this situation. Capillary pressure becomes the major force driving fluid flow in unsaturated concretes at low hydraulic pressures. Porous ITZs slow the full saturation of pores in this scenario. Under capillary pressure, aggregates without ITZs increase the fluid flow time compared to the pure mortar but have no effect on fluid flow under hydraulic pressure.

The fluid flow is fastest when the external pressure is horizontal, and it is slowest when the external pressure is vertical. As the gas volume content increases, the full saturation process takes longer.

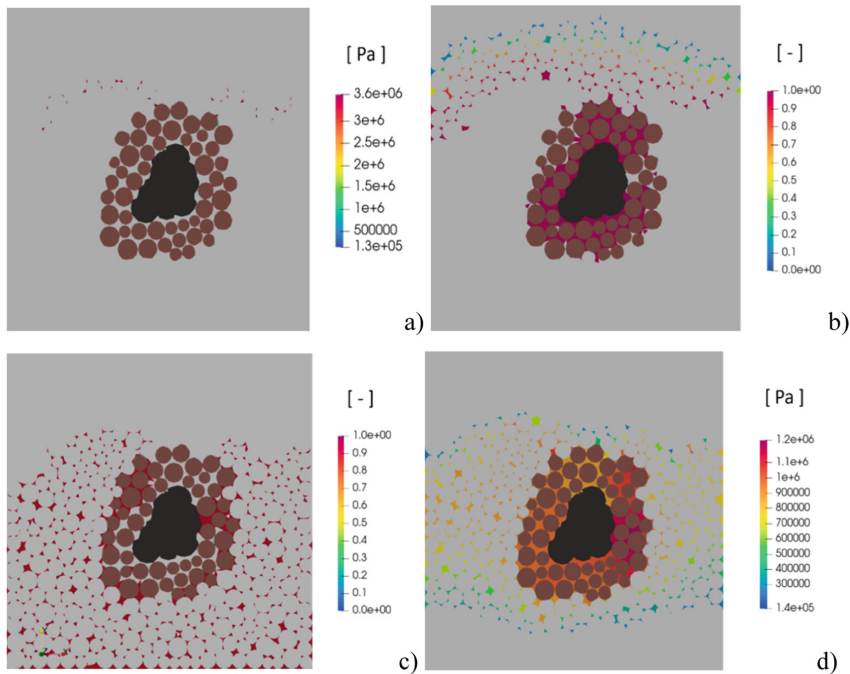


Fig. 4. Computation results of capillary-driven fluid flow in mortar specimen with aggregate and ITZ: (a) capillary pressure, (b) water phase fraction, (c) water saturation state and (d) high hydraulic pressure zone

Acknowledgements. The present study was supported by the research project “Fracture propagation in rocks during hydro-fracking—experiments and discrete element method coupled with fluid flow and heat transport” (years 2019–2022) financed by the National Science Centre (NCN) (UMO-2018/29/B/ST8/00255).

References

1. Bentz, D.P., Stutzman, P.E., Garboczi, E.J.: Experimental and simulation studies of the interfacial zone in concrete. *Cem. Conc. Res.* **22**(5), 891–902 (1992)
2. Li, K., Stroeven, P., Stroeven, M., Sluys, L.J.: A numerical investigation into the influence of the interfacial transition zone on the permeability of partially saturated cement paste between aggregate surfaces. *Cem. Concr. Res.* **102**, 99–108 (2017)
3. Krzaczek, M., Nitka, M., Kozicki, J., Tejchman, J.: Simulations of hydro-fracking in rock mass at meso-scale using fully coupled DEM/CFD approach. *Acta Geotech.* **15**(2), 297–324 (2019). <https://doi.org/10.1007/s11440-019-00799-6>
4. Krzaczek, M., Nitka, M., Tejchman, J.: Effect of gas content in macro-pores on hydraulic fracturing in rocks using a fully coupled DEM/CFD approach. *Int. J. Numer. Anal. Meth. Geomech.* **45**(2), 234–264 (2021)
5. Kozicki, J., Donzé, F.V.: A new open-source software developer for numerical simulations using discrete modeling methods. *Comput. Methods Appl. Mech. Eng.* **197**, 4429–4443 (2008)

6. Nitka, M., Tejchman, J.: A three-dimensional meso scale approach to concrete fracture based on combined DEM with X-ray μ CT images. *Cem. Concr. Res.* **107**, 11–29 (2018)
7. Suchorzewski, J., Tejchman, J., Nitka, M.: Discrete element method simulations of fracture in concrete under uniaxial compression based on its real internal structure. *Int. J. Damage Mech* **27**(4), 578–607 (2018)
8. Suchorzewski, J., Tejchman, J., Nitka, M.: Experimental and numerical investigations of concrete behaviour at meso-level during quasi-static splitting tension. *Theoret. Appl. Fract. Mech.* **96**, 720–739 (2018)
9. Washburn, E.W.: The dynamics of capillary flow. *Phys. Rev.* **17**, 273 (1921)
10. Abdi, R., Krzaczek, M., Tejchman, J.: Comparative study of high-pressure fluid flow in densely packed granules using a 3D CFD model in a continuous medium and a simplified 2D DEM-CFD approach. *Granular Matter* **24**(1), 1–25 (2021). <https://doi.org/10.1007/s10035-021-01179-2>
11. Nitka, M., Tejchman, J.: Meso-mechanical modelling of damage in concrete using discrete element method with porous ITZs of defined width around aggregates. *Eng. Fract. Mech.* **231**, 107029 (2020)
12. Zamani, S., Kowalczyk, R.M., McDonald, P.J.: The relative humidity dependence of the permeability of cement paste measured using GARField NMR profiling. *Cem. Concr. Res.* **57**, 88–94 (2014)
13. Kameche, Z.A., Ghomari, F., Choinska, M., Khelidj, A.: Assessment of liquid water and gas permeabilities of partially saturated ordinary concrete. *Constr. Build. Mater.* **65**, 551–565 (2014)
14. Hall, C.: Water sorptivity of mortars and concretes: a review. *Mag. Concr. Res.* **41**(147), 1–61 (1989)